Applied Energy 306 (2022) 118069

Contents lists available at ScienceDirect

Applied Energy

journal homepage: www.elsevier.com/locate/apenergy

Optimal techno-economic energy management strategy for building's microgrids based bald eagle search optimization algorithm

Seydali Ferahtia [a], Hegazy Rezk [b,c,*], Mohammad Ali Abdelkareem [c,d,e], A.G. Olabi [d,e,f]

[a] Laboratoire d'Analyse des Signaux et Systémes, Dept. of Electrical Engineering, University of M'sila, Algeria
[b] College of Engineering at Wadi Addawaser, Prince Sattam Bin Abdulaziz University, Saudi Arabia
[c] Faculty of Engineering, Minia University, Egypt
[d] Dept. of Sustainable and Renewable Energy Engineering, University of Sharjah, P.O. Box 27272, Sharjah, UAE
[e] Sustainable Energy & Power Systems Research Centre, RISE, University of Sharjah, P.O. Box 27272, Sharjah, UAE
[f] Mechanical Engineering and Design, Aston University, School of Engineering and Applied Science, Aston Triangle, Birmingham B4 7ET, UK

HIGHLIGHTS

- Proposing an energy management strategy for a renewable-based microgrid.
- Minimum total operating cost is achieved successfully.
- The bus voltage has been stabilized employing a flat controller.
- Comprehensive analysis and statistics have been provided.

ARTICLE INFO

Keywords:
Microgrids
Energy management strategy
Energy efficiency
Modern optimization

ABSTRACT

This research proposes an effective energy management strategy (EMS) for the economic operation under standalone and grid-connected operating modes of integrated solar renewables microgrid. The proposed microgrid is composed of a photovoltaic generator (PV), a fuel cell system (FC), and a battery storage system. The random nature of the renewable and the load power imposed some stability problems and economic problems, including operating costs. The suggested technique was based on the bald eagle search optimization algorithm (BES), which was designed for a one-day scheduling horizon. The key objectives of this paper were to satisfy the load power with the lowest operating costs under a stable direct current (DC) bus voltage, enhance the overall system efficiency and protect the battery from deep discharge and overcharge. To demonstrate the effectiveness of the proposed strategy, the obtained results were compared with other optimizers, including particle swarm optimization (PSO), salp swarm algorithm (SSA), artificial eco-system optimizer (AEO), COOT optimizer, and political optimizer (PO). The comparison confirmed the superiority of the proposed strategy in terms of minimum operating energy cost (0.1577c€/kW), high efficiency (87.395%) and final SoC (33.268%).

1. Introduction

In the last decades, the penetration of distributed renewable energy into distribution networks has increased rapidly. However, their dependence on geographical and meteorological circumstances has imposed several challenges on the control and the management [1]. Contrarily, the integration of controllable sources, such as fuel cells (FC), microturbines (MT), and storage systems, including batteries, has a power system with more controllability. Nevertheless, the combination of various sources, including renewables, may regardless lead to coordination and controllability problems. Microgrid technology provides significant solutions for these problems and provides more advantages, including: minimizing the power peaks and fluctuations [2] and the ability to integrate artificial intelligence (IA) within the microgrids control and management systems [3].

Microgrids are low voltage autonomous clusters, composed of renewable and fossil energy sources and storage systems that fulfill a local establishment or community [4]. Energy storage systems (ESS), on

* Corresponding author.
E-mail address: hr.hussien@psau.edu.sa (H. Rezk).

https://doi.org/10.1016/j.apenergy.2021.118069
Received 8 August 2021; Received in revised form 4 October 2021; Accepted 12 October 2021

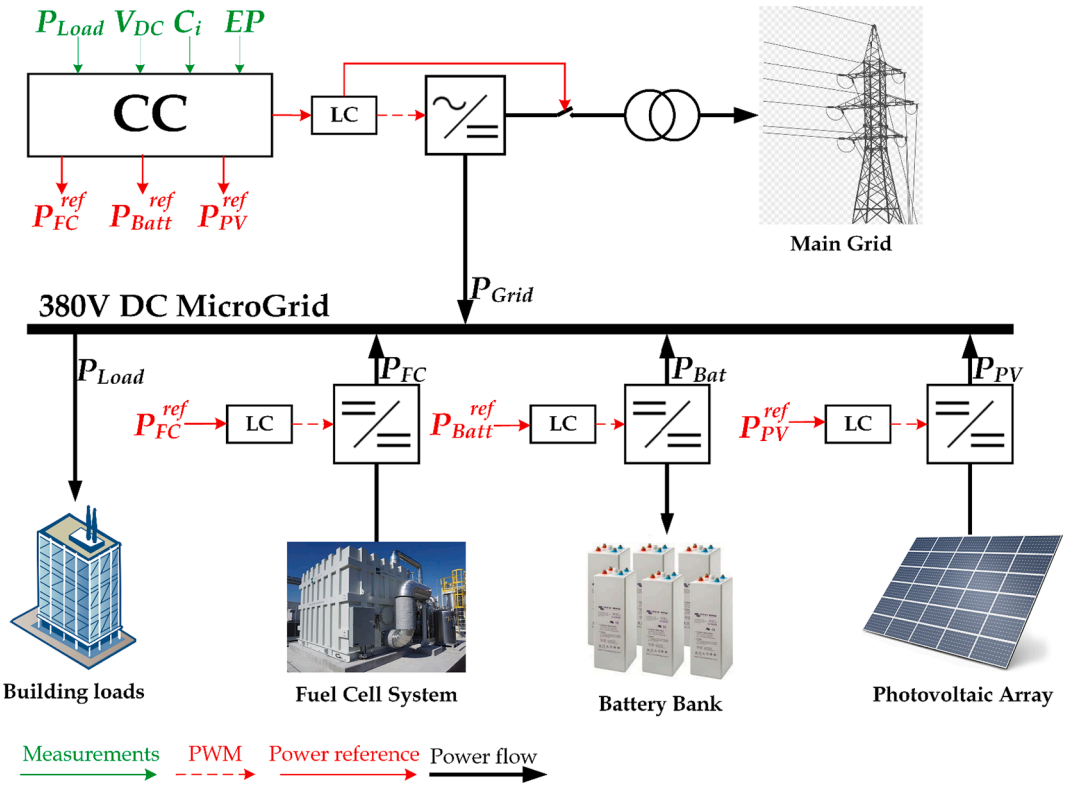

Fig. 1. The Proposed MG Topology including the power sources, the main grid, the CC and the LCs.

the other hand, play an essential role in supporting renewable sources and adding flexibility and controllability to their operation [5]. However, for commercial buildings with high consumption and low local renewable production, the combination of renewable sources and storage systems is not enough. For this reason, the integration of backup support systems is necessary. Diesel generators have been used widely as a backup support system; however, they have several disadvantages: low efficiency, pollutant emissions, and expensive operating and maintenance cost [6]. Hydrogen fuel cells may provide better performance as a backup system, due to their considerable advantages, including: low operating costs and maintenance, calm operating, and clean emissions [7].

To maximize the benefits of MG, such as improved economics and decreased main grid dependence, a suitable control system architecture must be employed. Hierarchical control is one of the most used strategies to control the MGs [8]. A typical MG hierarchical control system consists of two levels: local controllers (LCs) to control the power electronic interface of each source, and the central controller (CC) that generates the power references for each LC based on the embedded energy management strategy (EMS) and the current measures [9].

The main objective of combining these resources within the microgrid is to meet the commercial building's electrical loads, including heating, lighting, and cooling. To fulfil the consumption and production balance, techno-economic restrictions must be considered [10]. In general, the conception, design, and optimization of microgrids are attractive subjects. The technical issues have been presented in several papers, where the objective was to control some variables of the system, including the DC bus voltage, the storage system state-of-charge (SoC), fuel level, or system emissions. Other works presented economic strategies, where the objective was to decrease overall running and maintenance costs. Drop control strategy [11], hierarchical control strategy [12], and master-slave strategy [13] have been used widely in these fields.

Many academics have concentrated their studies on formulating the EMS and creating effective solutions to optimizing it. Two main categories of MG's EMS have been analyzed. These categories are: deterministic and probabilistic [14]. The deterministic EMSs are constructed based on prior knowledge, and the data inputs are assumed known. However, due to the fluctuation of renewable sources and market prices, the probabilistic EMSs provide better performance. A simple management strategy was presented in [15] for a standalone WT/PV/FC system. This strategy employed comprehensive dynamic models to evaluate their effects on system behavior. Hybrid model predictive control and rule-based control strategies were proposed in [16] for PV/FC grid-connected to reduce CO_2 emissions. A technical rule-based EMS was presented in [17] for a WT/PV/FC/SC microgrid. An economic EMS was proposed in [18] for a PV/WP/ESSs power system. Hatziargyriou et al. [19] proposed a coordinated operation of various distributed generation (DG) units and storage systems, regarding the economic benefits and power losses. An optimal techno-economic EMS for WT/PV/FC/Battery power system was presented in [20].

The metaheuristic algorithms (MAs) are receiving increased attention because of their high performance with stochastic problems. EMSs based on metaheuristic population-based optimization methods are gaining more attention. Genetic algorithm (GA) based EMS was proposed by Mohamed and Koivo [21] to minimize emissions costs (CO_2, SO_2, and NOx), installation costs, and operating and maintenance costs. A multi-objective adaptive modified particle swarm optimization algorithm (MAMPSO) was studied and implemented for a typical MT/FC/Battery MG with renewable energy sources [22]. Improved gravitational search algorithm (GSA) based EMS's were proposed by Li et al. [23] to optimize fuel consumption, operation and maintenance costs while also reducing pollutant emissions. Salp swarm algorithm (SSA) was used in [24] to enhance the power quality of a DC microgrid. The same algorithm was implemented in [25] to update the LQR parameters of a battery/supercapacitor power system.

However, because of the stochastic nature of the metaheuristic algorithms, each strategy may provide a different performance based on the embedded optimization algorithm. For this reason, this paper evaluated the performance of modern optimizers from both technical and

economic points of view. This paper presented a techno-economic EMS for a PV/FC/Battery grid-connected LV DC microgrid. The main contributions of this paper are listed as follows:

- Design an optimized techno-economic energy management strategy (EMS) for a DC microgrid that responds to commercial building energetic requirements with optimal operating costs.
- Optimization of the microgrid operating cost employing the blade eagle search algorithm on the EMS, the physical limitations of each power source are included such as the battery limitations.
- Enhance the stability and provide power quality using the flatness control approach.
- Enhance the power system overall efficiency.

The studied power system topology is presented in Fig. 1. The proposed EMS was based on the bald eagle search optimization algorithm (BES). The proposed strategy was compared with other metaheuristic algorithms (MAs) to confirm its performance. The used algorithms were: particle swarm optimization (PSO), salp swarm algorithm (SSA), political optimizer (PO), artificial eco-system optimizer (AEO), and Coot optimization algorithm (COOT). The DC bus voltage was stabilized using the flatness control strategy. Controlling and optimizing the microgrids was a typical multi-objective problem that included various MG issues, such as: stability, cost, fuel consumption, safety, and efficiency. This paper focused on reducing the total operating cost under stable bus voltage. A single objective optimization strategy that included operation costs was used to reduce the operating costs, where the stabilization strategy was performed utilizing a flatness control strategy.

The rest of the paper was structured as follows: Section 2 presented the power system description. The proposed EMS was explained in Section 3; this section included the objective function formulation and the DC voltage stabilization control law. Section 4 explained the optimization algorithms. The results and discussion were presented in Section 5. The paper then ended with a conclusion in Section 6.

2. Power system description

Fig. 1 shows the typical grid-connected low-voltage (LV) microgrid, consisting of several types of DG: FC system, PV array, Li-ion battery storage system, and building loads. The microgrid can exchange the power with the main grid (MV distribution grid) through an MV/LV transformer and bidirectional DC/AC converter. A boost converter was used to control the PV and the FC system. A bidirectional buck/boost converter was utilized to control the battery power. A bidirectional DC/AC converter was used to manage the exchanged power with the main grid. All of the power sources were connected to a 380 V dc common bus via their power converters. Each converter was controlled using their local controller (LC), which generated the PWM signal based on the received power reference from the central controller (CC).

From Fig. 1, the available energy on the DC bus (E_{bus}) can be expressed as a function of the exchanged power as follows:

$$\dot{E}_{bus} = P_{PV} + P_{FC} + P_{Batt} + P_{Grid} - P_{Load} \tag{1}$$

where P_{PV}, P_{FC}, and P_{Batt}, are PV, FC and battery output power, P_{Load} is the load power and P_{Grid} is the Grid power. The dc bus energy can be expressed as follows:

$$E_{bus} = \frac{C_{bus}}{2} V_{bus}^2 \tag{2}$$

where V_{bus} is the bus voltage and C_{bus} is the bus capacity.

3. The proposed EMS

An energy management strategy (EMS) was implemented on the CC to optimize the operation of the microgrid following the electricity prices (EP), the power sources operating costs (C_i), and predicted load power. Moreover, the EMS had to ensure power quality and stability.

3.1. Objective function formulation

The PV generator as a free energy source operated at its maximum power point (MPP). As such, its power reference was generated using an MPPT algorithm. The PV power was injected directly to supply to the load. However, the demanded power was considerably higher than the generated PV power, meaning the deficit power was supplied by all of: the FC, the battery, and the grid power according to the EMS decisions.

If the load power exceeded the generated power by the microgrid's power sources or if the power sources operating cost was higher, the microgrid turned on on-grid mode, and the load was mainly supplied by the grid power, considering the economic gains. This objective can be formulated as an optimization problem that minimized the operating cost. The optimization problem can be expressed and defined in the objective function as follows:

$$\begin{aligned} F_{Cost} &= min\left(\sum_{t=1}^{T}\sum_{i=1}^{N}\left(C_i(P_{Gi}(t)) + P_{Grid}(t).EP(t)\right)\Delta T\right) \\ &= min\left(\sum_{t=1}^{T}\left(C_{FC}(P_{FC}(t)) + C_{Batt}(P_{Batt}(t)) + P_{Grid}(t).EP(t)\right)\Delta T\right) \end{aligned} \tag{3}$$

where N is the number of power sources and T is the total number of time intervals; P_{Gi} is the i-th DG power; C_i, C_{FC} and C_{Batt} are the i-th DG, the FC, the battery operating costs; $EP(t)$ is the electricity market prices at time t; ΔT is the sampling time.

This function was submitted to several constraints, such as the power balance and the power generation capacity.

3.2. Constraints

Assuming that losses in the microgrid were neglected, the total power generated by the power sources must be equal to the load power for each time interval, t. Therefore, the power balance constraint can be described as follows:

$$\begin{aligned} P_{Load} &= \sum_{i=1}^{N} P_{Gi} + P_{Grid} \\ &= P_{PV} + P_{FC} + P_{Bat} + P_{Grid} \end{aligned} \tag{4}$$

Moreover, each generation unit has its physical production capacity. As such, it has to provide the power within its range as follows:

$$P_{Gi}^{min} \leqslant P_{Gi} \leqslant P_{Gi}^{max} \tag{5}$$

According to, each generator operating cost is a considered quadratic relationship that can be expressed as follows:

$$C_i = (a_i P_{Gi})^2 + b_i P_{Gi} + c_i \tag{6}$$

where a_i, b_i, and c_i are the cost coefficients.

Thus, the objective function has constraints on the power generators, where the battery and the FC have their output limitations; these constraints are presented as follows:

$$P_{FC}^{min} \leqslant P_{FC} \leqslant P_{FC}^{max} \tag{7}$$

$$P_{Batt}^{min} \leqslant P_{Batt} \leqslant P_{Batt}^{max} \tag{8}$$

$$P_{Grid} = P_{Load} - (P_{FC} + P_{Batt}) \tag{9}$$

where P_{FC}^{min} and P_{FC}^{max} are the FC min and max output power, P_{Batt}^{min} and P_{Batt}^{max} are the max charging and discharging power, respectively.

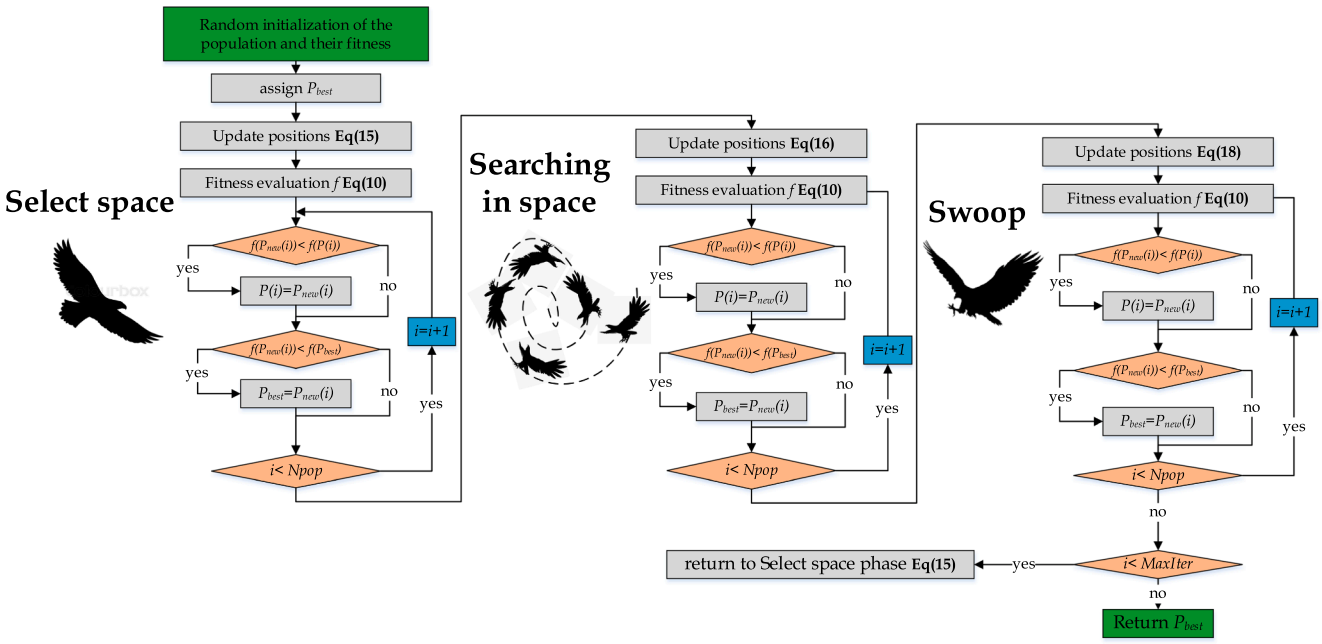

Fig. 2. BES Optimization Algorithm flowchart includes the three optimization stages: selecting space, searching in space and swooping.

3.3. Storage system requirements

The battery shared its energy with the microgrid, according to the power reference generated by EMS. However, for many papers that proposed an economic EMS, the battery state of charge (SoC) was not included in the EMS. To avoid the battery's deep discharge or overcharge, the EMS had to include the SoC in the objective function. In this paper, the battery SoC was considered on the objective function as follows:

$$F_{Cost} = min(\sum_{t=1}^{T}(C_{FC}(P_{FC}(t)) + C_{Batt}(P_{Batt}(t)).(SoC(t) - SoC_{opt})^2 + P_{Grid}(t).EP(t))\Delta T) \quad (10)$$

where SoC_{opt} is the optimal SoC.

In this study, the optimization variables were the power reference for each generator, including the main grid power reference. However, according to Eq. (9), the main grid power reference was unconsidered as an optimization variable to ensure the power balance in Eq. (4).

The optimization problem was resolved by means of a recent meta-heuristic algorithm called bald eagle search optimization algorithm.

3.4. DC bus voltage stabilization

Mainly, the load was supplied by the PV, the FC, and the main grid power, where the main function of the battery was to stabilize the DC bus voltage by supplying the transient periods. The voltage can be stabilized using the flatness control strategy; this strategy provided excellent performance as obtained in [26], where battery power reference was obtained from Eq. (11) as follows:

$$P_{Batt}^{ref} = \dot{E}_{bus}^{req} + P_{Load} - P_{PV} - P_{FC} - P_{Grid} \quad (11)$$

where $\dot{E}_{bus}^{req}$ is the required power by the common bus, it can be obtained based on the second-order trajectory generation equation as follows:

$$\frac{d(E_{bus} - E_{bus}^{ref})}{dt} + k_1(E_{bus} - E_{bus}^{ref}) + k_2\int_0^t (E_{bus} - E_{bus}^{ref})dt = 0 \quad (12)$$

where k_1 and k_2 are the trajectory generation coefficients. These coefficients can be obtained as follows:

$$k_1 = 2\zeta\omega_n \quad (13)$$

$$k_2 = \omega_n^2 \quad (14)$$

where ξ is the damping coefficient (0.707) and ω_n is the cutoff frequency.

4. Optimization mechanism

4.1. Bald eagle search optimization algorithm:

BES is a new nature-inspired meta-heuristic optimization algorithm that imitates bald eagle hunting behavior [27]. This algorithm has three stages. In the first stage (selecting space), the bald eagle chooses the best area in terms of food amount. In the second stage (searching in space), the eagle searches for prey inside the designated area. From the best-obtained position in the second step, the eagle swings to determine the optimum hunting site in the third stage (swooping).

a. Selection space: In this stage, new positions will be generated according to the following equation:

$$P_{new}(i) = P_{best} + \alpha.r.(P_{mean} - P(i)) \quad (15)$$

where $P_{new}(i)$ is the i-th newly generated position, P_{best} is the best-obtained position, P_{mean} is the mean position, α is a control gain [1.5, 2], and r is a random number [0, 1]. The fitness of each new position will

be evaluated, if any new position (P_{new}) provides a better fitness compared with the provided by the P_{best}, this new position will be assigned as P_{best}.

b. Searching in space: after the assignment of the best search space (P_{best}), the algorithm updates the position of the eagles inside this search space. The updating model is formulated as follows:

$$P_{new}(i) = P(i) + y(i).(P(i) - P(i+1)) + x(i).(P(i) - P_{mean}) \tag{16}$$

where $P_{new}(i)$ is the i-th newly generated positions, P_{mean} is the mean position, x and y are directional coordinates for the i-th position, they can be defined as:

$$\begin{aligned} x(i) &= \frac{xr(i)}{max(|xr|)};\ \ xr(i) = r(i).sin(\theta(i)) \\ y(i) &= \frac{yr(i)}{max(|yr|)};\ \ yr(i) = r(i).cos(\theta(i)) \\ \theta(i) &= a.\pi.rand;\ \ r(i) = \theta(i).R.rand \end{aligned} \tag{17}$$

where a is a control parameter that used for determining the corner between point search in the central point, it takes value in [5, 10], R is a parameter in [0.5, 2] used to determine the number of search cycles. The fitness of the new positions will be evaluated, and the P_{best} value will be updated according to the obtained results.

c. Swooping: in this stage, eagles move toward the target prey from the best-obtained position. The hunting model is presented as follows:

$$P_{new}(i) = rand.P_{best} + x1(i).(P(i) - c_1.P_{mean}) + y1(i).(P(i) - c_2.P_{best}) \tag{18}$$

where c_1 and c_2 are random numbers [1,2]; $x1$ and $y1$ are directional coordinates, they can be defined as

$$\begin{aligned} x1(i) &= \frac{xr(i)}{max(|xr|)};\ \ xr(i) = r(i).sinh(\theta(i)) \\ y1(i) &= \frac{yr(i)}{max(|yr|)};\ \ yr(i) = r(i).cosh(\theta(i)) \\ \theta(i) &= a.\pi.rand;\ \ r(i) = \theta(i) \end{aligned} \tag{19}$$

Fig. 2 was presented to give more visibility and readability to this algorithm, where *Npop* is the number of positions (population size), and *MaxIter* is the max number of iterations.

4.2. Particle swarm optimization:

The PSO is a stochastic optimization method based on the collective conduct of certain animal's swarms, such as birds' flock or fish schools [28]. This behavior can be modeled as follows:

$$\begin{aligned} V_i^{t+1} &= \omega V_i^t + c_1^{PSO} r_1 (pbest_i - X_i^t) + c_2^{PSO} r_2 (gbest_i - X_i^t) \\ X_i^{t+1} &= X_i^t + V_i^{t+1} \end{aligned} \tag{20}$$

where V_i^{t+1} and X_i^{t+1} are velocity and the position of the i-th agent at instant $t+1$, w is the inertia weight constant, c_1^{PSO} and c_2^{PSO} are the self-knowledge and group knowledge weights- also known as correction factors- r_1, r_2 are random numbers [0, 1], t is the iteration.

4.3. Salp swarm algorithm

SSA is a bio-inspired algorithm inspired by the movement of the salps on the ocean [29]. In the SSA population, there are two types of salps: leaders and followers. The mathematical model that describes the leaders (LP) and the followers' positions (FP) at instant t is formulated as follows:

$$\begin{aligned} LP(t) &= \begin{cases} FP(t) + c_1^{SSA}((ub^{SSA} - lb^{SSA})c_2^{SSA} + lb^{SSA}) & c_3^{SSA} < 0.5 \\ FP(t) - c_1^{SSA}((ub^{SSA} - lb^{SSA})c_2^{SSA} + lb^{SSA}) & c_3^{SSA} > 0.5 \end{cases} \\ c_1^{SSA} &= 2e^{-(4t/T_{max})^2} \\ FP_i(k) &= 0.5(FP_i(k-1) + FP_{i-1}(k)) \end{aligned} \tag{21}$$

where c_2^{SSA} and c_3^{SSA} represent random numbers [0, 1]. ub^{SSA} and lb^{SSA} are the upper and the lower search space limits; T_{max} is the max number of iterations.

4.4. Artificial eco-system optimizer

AEO is a novel meta-heuristic optimization algorithm inspired by living organisms' behaviors [30]. Living organisms have three stages: production, consumption, and decomposition. The production operator model can be represented at the iteration $t+1$ as:

$$\begin{aligned} x_1^{t+1} &= (1-a)x_n^t + ax_{ran}^t \\ a &= (1 - t/Tmax)r_1^{AEO} \\ x_{rand} &= r(ub^{AEO} - lb^{AEO}) + lb^{AEO} \end{aligned} \tag{22}$$

where x_1^{t+1} represents the first agent position at iteration t + 1, r_1^{AEO} is a random number [0, 1], r is a random vector [0, 1] and x_{rand} is a set of random positions.

The consumption behavior can be modeled according to the living type. If the living is an herbivore, its model can be formulated as:

$$\begin{aligned} x_i^{t+1} &= x_i^t + C(x_i^t - x_1^t), \quad i \in [2, ..n] \\ C &= \frac{1}{2}\frac{v_1}{|v_2|}, \quad v_1 \sim N(0,1) \quad v_2 \sim N(0,1) \end{aligned} \tag{23}$$

where x_i^{t+1} is the i-th agent position at iteration $t+1$, C is Levy flight function and $N(0,1)$ denotes the normal distribution. *Political Optimizer*

PO is a recent optimization algorithm inspired by the phased stages of politics [31]. There are several phases in this optimizer: constituency allocation, party switching, election campaign, inter-party election, and parliamentary affairs. The exploration and exploitation are performed on the election campaign phase, and the updating model is presented as follows:

$$p_{i,k}^j(t+1) = \begin{cases} m^* + r(m^* - p_{i,k}^j(t)) & if \quad p_{i,k}^j(t-1) \leqslant p_{i,k}^j(t) \leqslant m^* \quad or \quad p_{i,k}^j(t-1) \geqslant p_{i,k}^j(t) \geqslant m^* \\ m^* + (2r-1)\left|m^* - p_{i,k}^j(t)\right| & if \quad p_{i,k}^j(t-1) \leqslant m^* \leqslant p_{i,k}^j(t) \quad or \quad p_{i,k}^j(t-1) \geqslant m^* \geqslant p_{i,k}^j(t) \\ m^* + (2r-1)\left|m^* - p_{i,k}^j(t-1)\right| & if \quad m^* \leqslant p_{i,k}^j(t-1) \leqslant p_{i,k}^j(t) \quad or \quad m^* \geqslant p_{i,k}^j(t-1) \geqslant p_{i,k}^j(t) \end{cases} \tag{24}$$

Table 1
System Paramaters.

Parameter	Value
DC Bus Voltage	380 V
FC max power	250 kW
Battery's capacity	1500 Ah
Max SoC	90%
Min SoC	30%

- Case 2: the target solution is located between the current and the previous position.
- Case 3: the previous position is located between the current position and the target solution.

Eq. (29) can be explained similarly.

$$p_{i,k}^{j}(t+1)=\begin{cases} m^{*}+(2r-1)\left|m^{*}-p_{i,k}^{j}(t)\right| & if\ p_{i,k}^{j}(t-1)\leqslant p_{i,k}^{j}(t)\leqslant m^{*}\ \ or\ \ p_{i,k}^{j}(t-1)\geqslant p_{i,k}^{j}(t)\geqslant m^{*} \\ p_{i,k}^{j}(t-1)+r(p_{i,k}^{j}(t)-p_{i,k}^{j}(t-1)) & if\ \ p_{i,k}^{j}(t-1)\leqslant m^{*}\leqslant p_{i,k}^{j}(t)\ or\ p_{i,k}^{j}(t-1)\geqslant m^{*}\geqslant p_{i,k}^{j}(t) \\ m^{*}+(2r-1)\left|m^{*}-p_{i,k}^{j}(t-1)\right| & if\ m^{*}\leqslant p_{i,k}^{j}(t-1)\leqslant p_{i,k}^{j}(t)\ \ or\ m^{*}\geqslant p_{i,k}^{j}(t-1)\geqslant p_{i,k}^{j}(t) \end{cases} \tag{25}$$

where r is a random [0, 1], and m^{*} first holds the value of the kth dimension of the party leader.

Both of these equations have three cases. The key objective of these cases is to determine and exploit the best region in the search space. The cases of Eq. (28) can be interpreted as follows:

- Case 1: the current position is located between its previous position and the target solution.

Table 2
Load and PV power characterestics.

Metric	Load power	PV power
Min power (kW)	12.43	0
Max power (kW)	268.9	170.4
Mean power (kW)	149.4	35.81
Median power (kW)	164.5	11.43
StD	84.69	46.87
Range	256.5	170.4

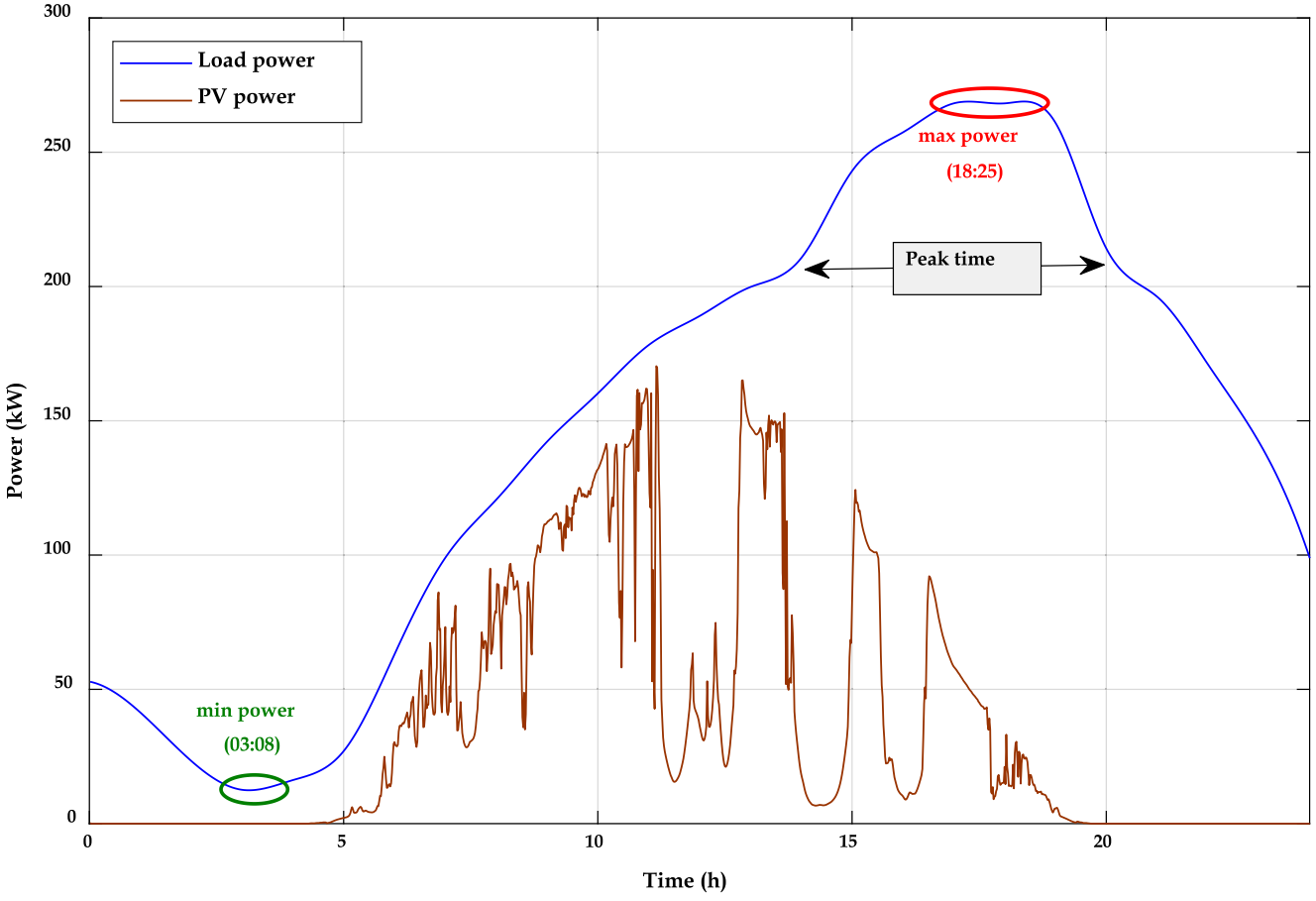

Fig. 3. The considered load and Solar Power Profiles.

Table 3
Optimizer Paramaters.

Parameter	Value
Number of agents	10
Max iterations	8
Number of variables	2
Number of runs	10

4.5. COOT optimizer

Coot is a novel meta-heuristic algorithm motivated by the movement of birds called Coot on the water surface [32]. There are two distinct types of birds in this population: leaders, and the other birds that update their positions (*CootPos*) according to the leaders' positions (*LeaderPos*). There are four stages in this optimizer:

(a) Random movement to this side and that side: the birds move randomly to explore the search space, this movement can be modeled as follow.

$$CootPos(i) = CootPos(i) + A \cdot R_2(Q - CootPos(i)) \qquad A = 1 - i/MaxIter \tag{26}$$

R_2 is a random number$\in [0,1]$, Q is a random position and *MaxIter* is the max number of iterations.

(b) Adjusting the position based on the group leaders: similar to the updating mechanism of the SSA algorithm, the COOT updates the birds' positions. Each bird updates its position following the previous bird position as:

$$CootPos_n(i) = 0.5 \cdot (CootPos_n(i) + CootPos_{n+1}(i)) \tag{27}$$

where $CootPos_n(i)$ is the n-th coot at instant i.

(c) Position updating based on the group leaders: the coots update their position according to the leaders' positions as follow

$$CootPos_n(i+1) = LeaderPos_n(i) + 2R_1 cos(2\pi R)(LeaderPos_n(i) - CootPos_n(i+1)) \qquad k = 1 + mod\ (n, N_{leader}) \tag{28}$$

where N_{leader} is the leaders' number, n is the search space dimension, R_1 is a random number$\in [0,1]$, R is a random number$\in [-1,1]$.

(d) Leading the group by the leaders towards the optimal area (leader movement): The leaders update their position as follows:

Table 4
Cost Coefficient for both FC and Battery.

Cost Coefficient	Value	Unit	Cost Coefficient	Value	Unit
a_{FC}	0	€ct/kWh^2	a_{Batt}	0	€ct/kWh^2
b_{FC}	0.294	€ct/kWh	b_{Batt}	0.38	€ct/kWh
c_{FC}	0	€ct/h	c_{Batt}	0	€ct/h

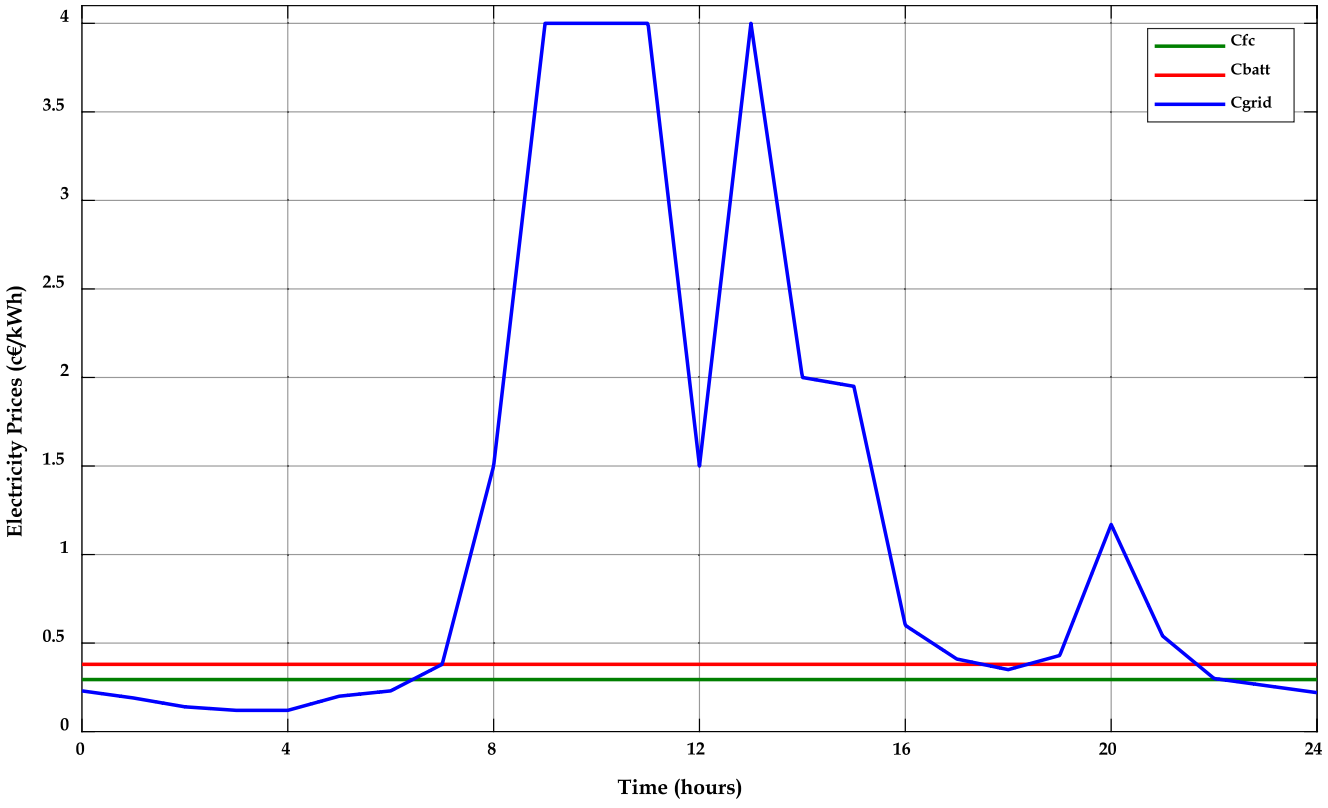

Fig. 4. The considered electricity Prices.

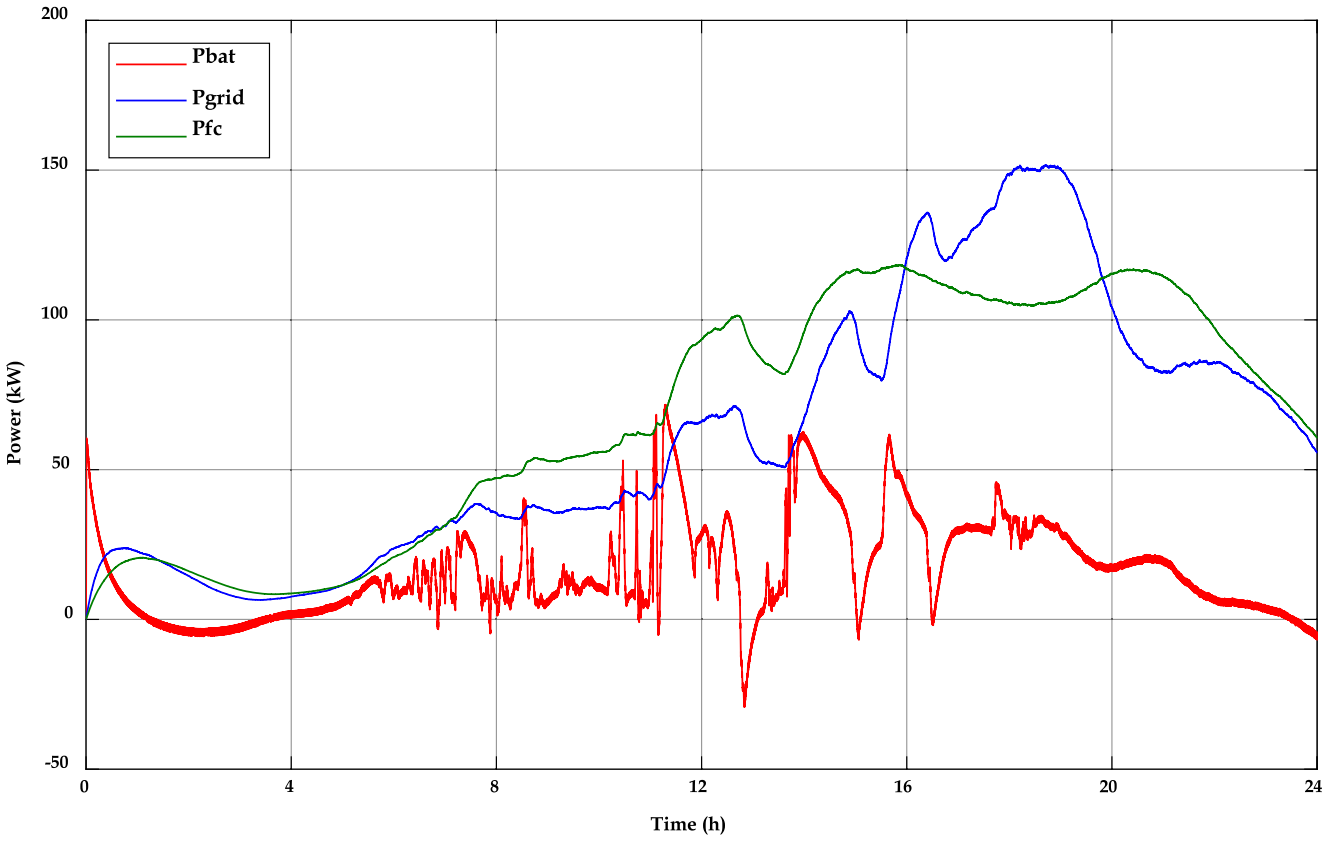

Fig. 5. The generated battery, grid and fuel cell power using the AEO.

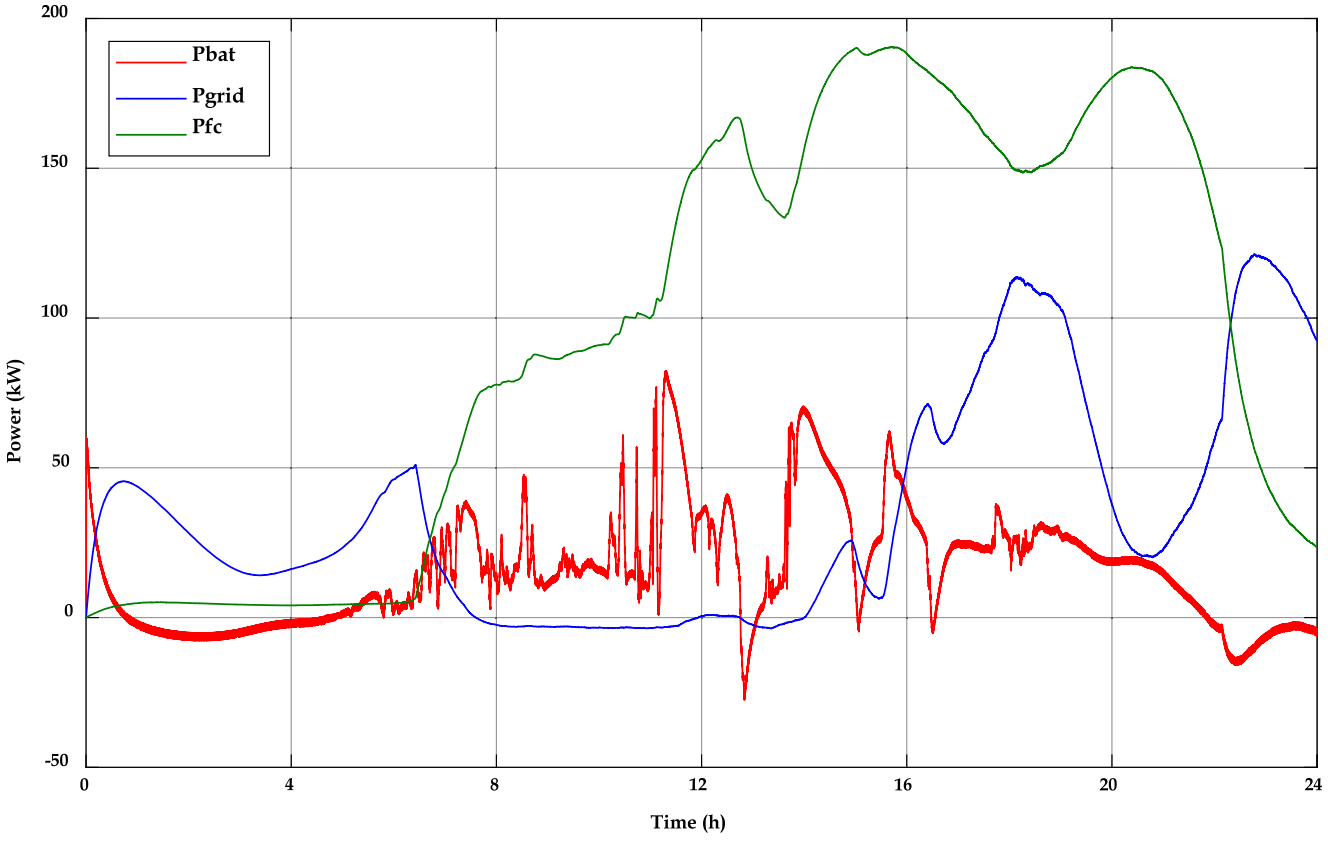

Fig. 6. The generated battery, grid and fuel cell power using the PO.

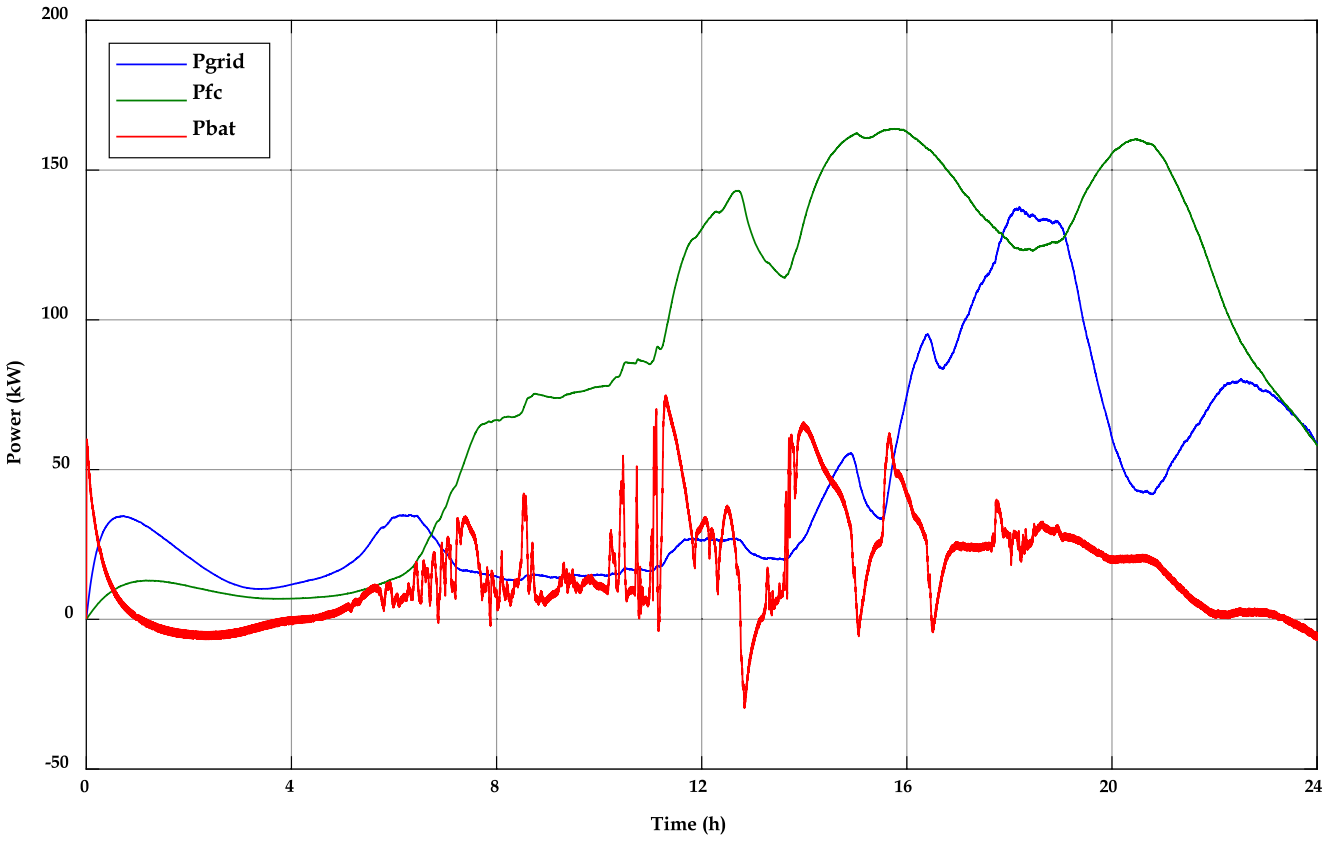

Fig. 7. The generated battery, grid and fuel cell power using the PSO.

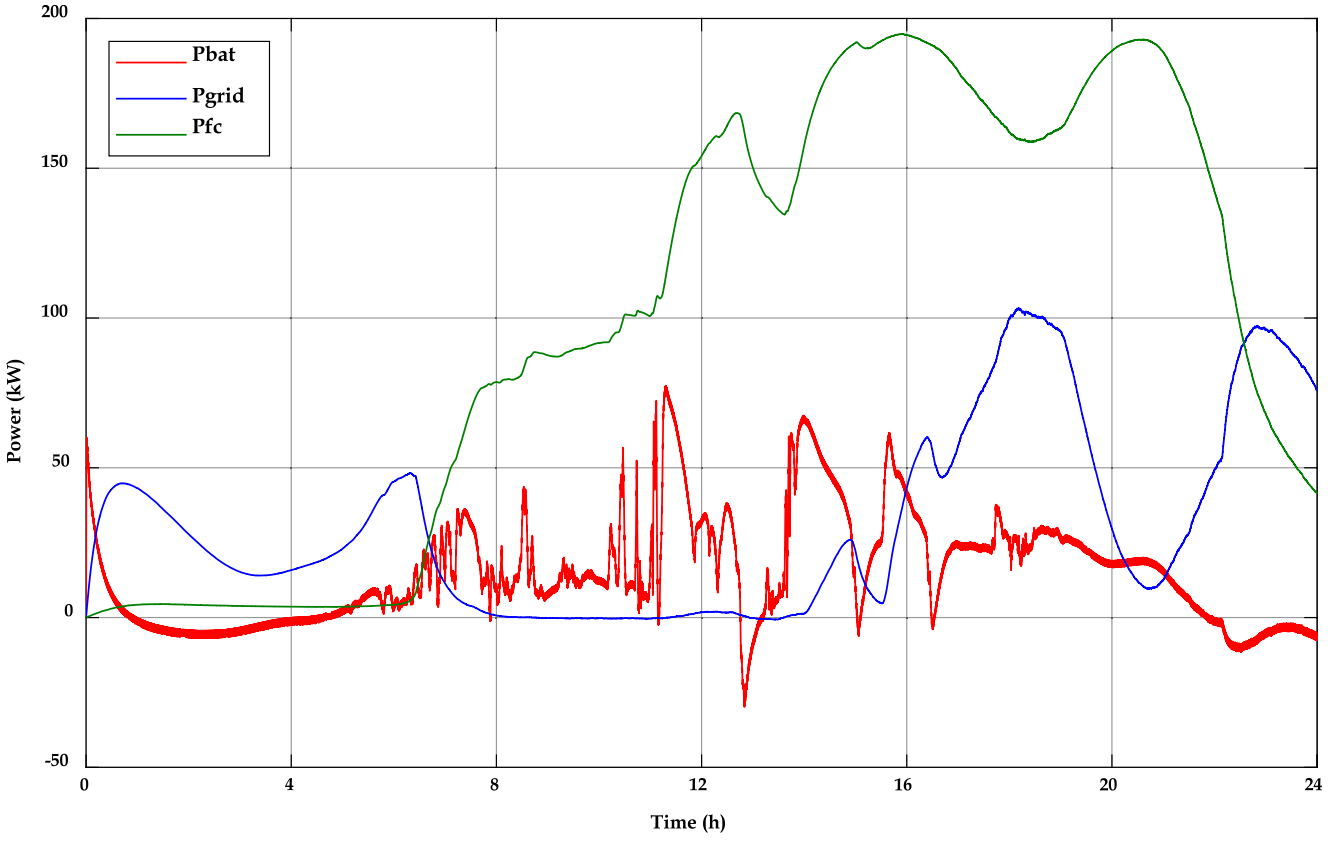

Fig. 8. The generated battery, grid and fuel cell power using the SSA.

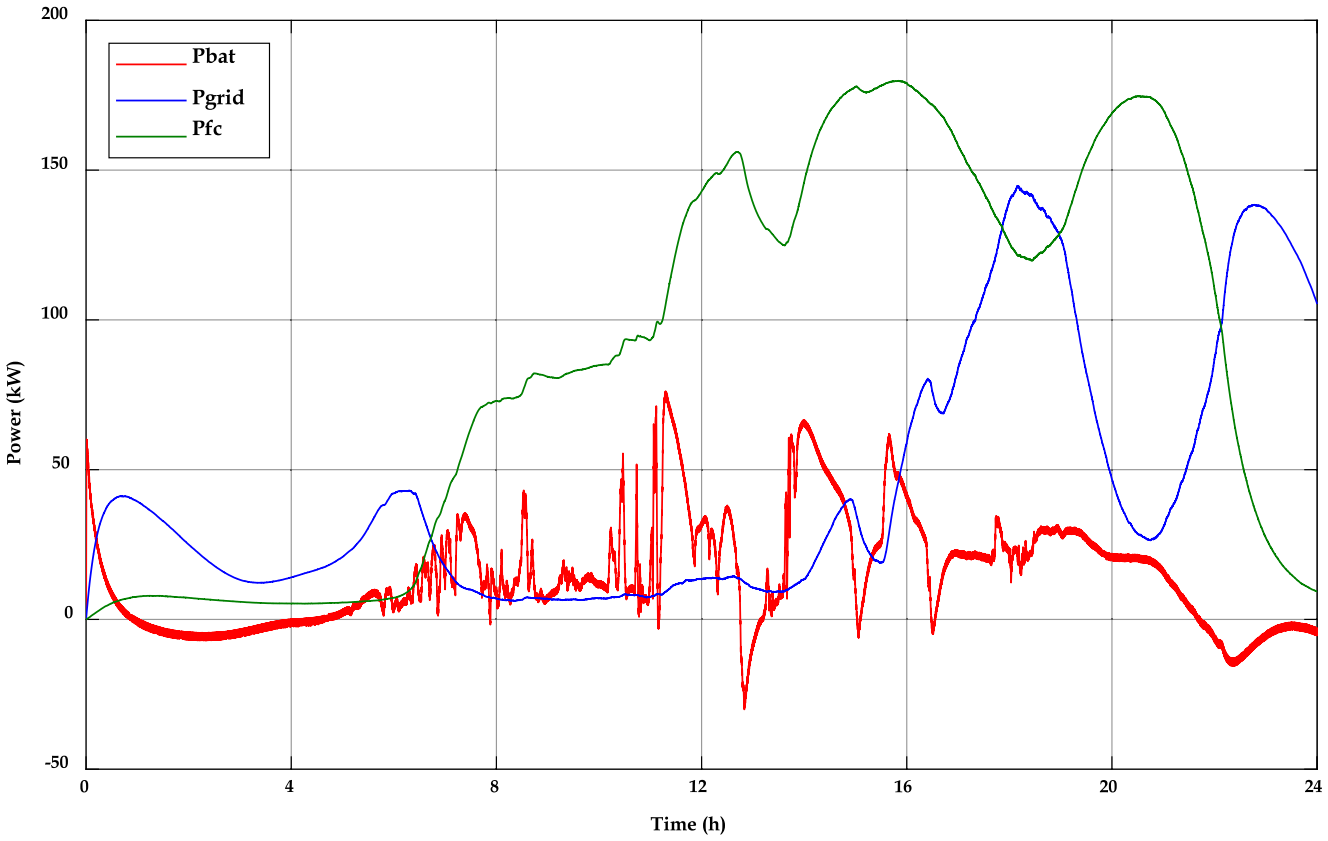

Fig. 9. The generated battery, grid and fuel cell power using the COOT.

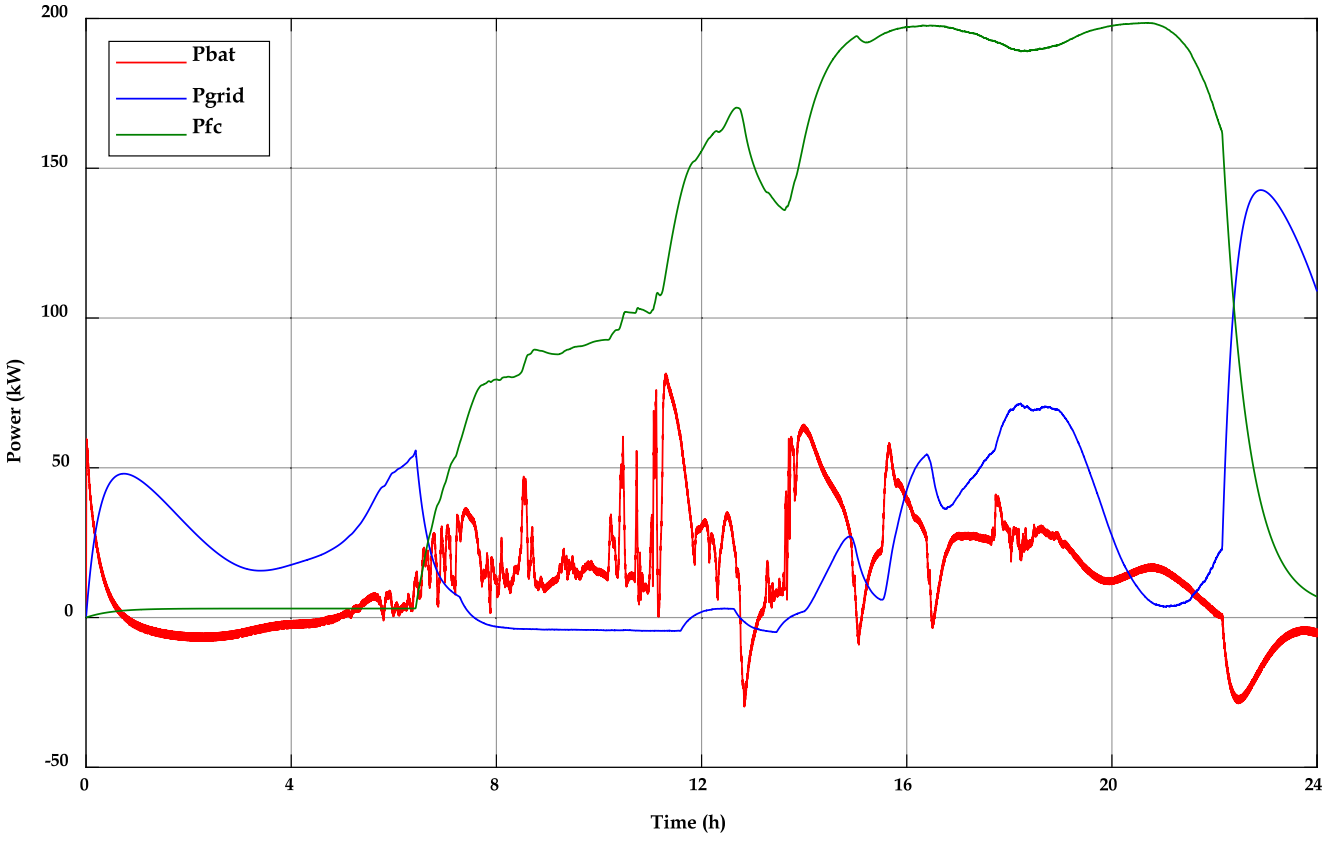

Fig. 10. The generated battery, grid and fuel cell power using the BES.

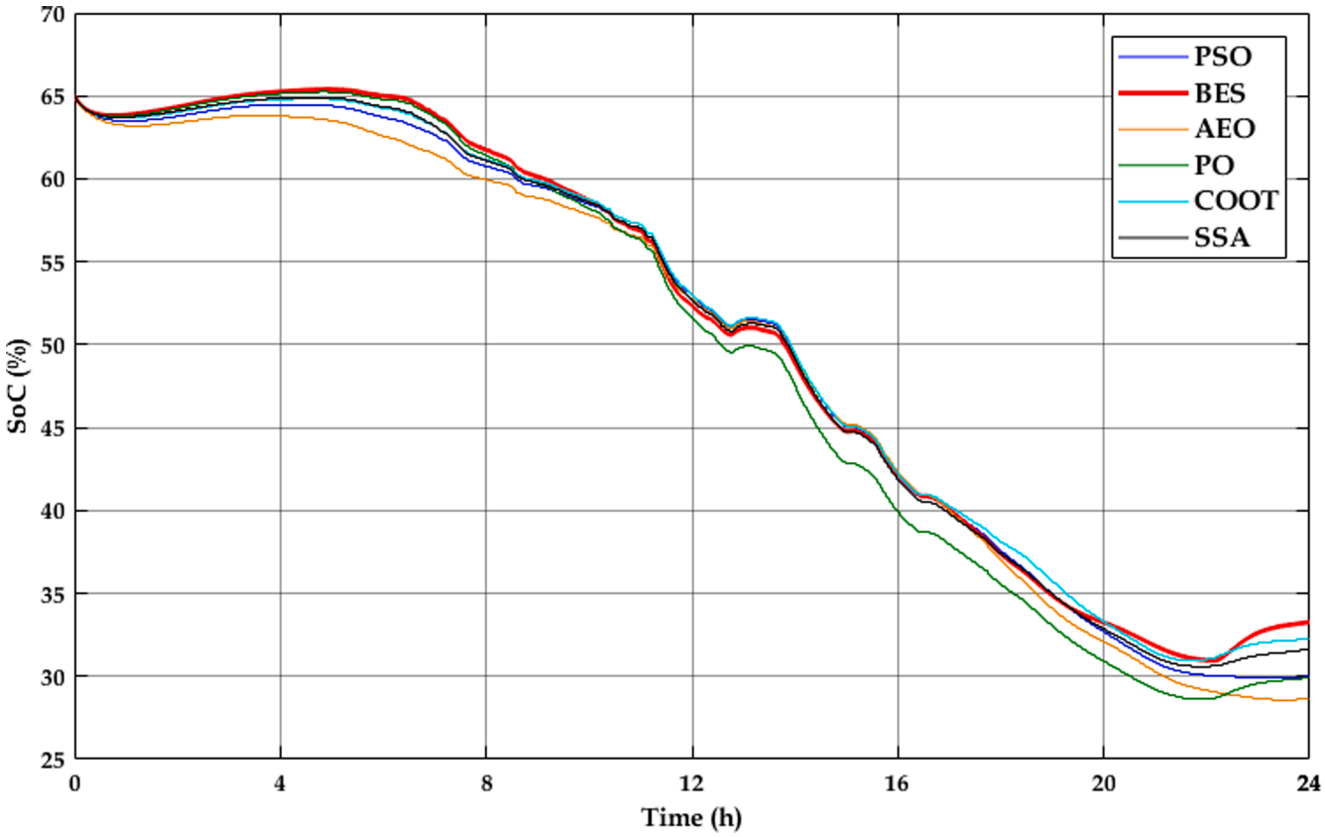

Fig. 11. The battery State of Charge (SoC) using all the algorithms (%).

$$LeaderPos_n(i)=\begin{cases} B\cdot R_3\cdot cos(2R\pi)\cdot(gBest-LeaderPos_n(i+1))+gBest\, R_3<0.5 \\ B\cdot R_3\cdot cos(2R\pi)\cdot(gBest-LeaderPos_n(i+1))-gBest\, R_3\geqslant 0.5 \end{cases}$$
$$B=2-{}^{i}/_{MaxIter} \tag{29}$$

where *gBest* is the best-obtained position, R_3 and R_4 are random numbers$\in[0,1]$, B is a converging factor that can be calculated as the above equation.

5. Results and discussion

To validate the performance of the proposed EMS, the microgrid was simulated under variable load and solar radiance. The system parameters are presented in Table 1. The typical solar and load power profiles are presented in Fig. 3, while their characteristics are provided in Table 2. The simulation parameters are presented in Table 3, and the cost parameters are presented in Table 2 and Fig. 4 [14] (see Table 4).

To evaluate the performance of the proposed EMS, it was compared with other popular and recent optimizers, including PSO, SSA, PO, AEO, and COOT.

As can be seen in Fig. 3, that the load power was much higher than solar power. As explained before, the deficient power was supplied by the FC, the battery, and the grid. The EMS assigned the power reference for each source. The obtained results are presented in Fig. 5 for the obtained results using AEO based EMS, Fig. 6 for the PO based EMS, Fig. 7 for the PSO based EMS, Fig. 8 for the SSA based EMS, Fig. 9 for the COOT based EMS, and Fig. 10 for the BES based EMS.

From Fig. 4, there are two main times: the low grid price, from 22:00 to 7:00. In this time, the grid power was cheaper than the FC and the battery power; at the other time: the low grid price, during the grid power cost was higher.

From these results, in the periods from 1 to 6 h and from 23 to 24 h, the main grid supplied a large portion of the load. This is because the electricity market was lower in comparison to power sources operating costs and the battery charge during this time. After 7:00, the FC supplied the load, while the battery supplied the transient periods caused by the weather fluctuations. The grid price dropped after 13:00; and the load power rose to reach its high level at 17:00. During this time, the FC supplied most of the load; the grid injected its power according to the prices, as displayed in the power figures. The battery shared its power according to the dc bus required power and the bus voltage. The exchanged battery power was expressed with its SoC, and the battery SoC is presented in Fig. 11. The simulation results and statistics, including: the efficiency, the final SoC, the mean operating cost, and the optimizer efficiency, are presented in Table 5.

The ANOVA statistics are presented in Table 6, and the *F* value was much higher than the *p*-value (critical value), which proved the variance between the optimizers' performance. Fig. 12 presents the ANOVA results for each optimizer. This figure demonstrated the robustness and the accuracy of the BES when compared with the other algorithms. However, the high complexity of the BES algorithm may be challenging for its hardware implementation. Moreover, the integration of other sources on the microgrid will certainly require more advanced computers for the real-world application due to the high complexity and computing time

Tukey HSD (honestly significant difference) test results are provided in Fig. 13. This test was used to confirm that the results' means were significantly different for each optimizer. From these results, the proposed BES had a significantly different mean from the other five optimizers.

The DC bus voltage was stabilized by the used flat controller, as displayed in Fig. 14. Voltage fluctuations were due to loads and solar power fluctuations. The solar profile used was taken from the cloudy day profile, and this profile was used to evaluate the durability of the controller.

Table 7 shows statistics on the DC bus voltage. From these results, the

Table 5
Simulation results.

	PSO		SSA		AEO		PO		COOT		BES	
Run	Sys. Efficiency (%)	Final SoC (%)	Sys. Efficiency (%)	Final SoC (%)	Sys. Efficiency (%)	Final SoC (%)	Sys. Efficiency (%)	Final SoC (%)	Sys. Efficiency (%)	Final SoC (%)	Sys. Efficiency (%)	Final SoC (%)
1	85.242	30.039	86,006	31.647	83.518	28.693	84.340	4.0415	85.974	32.264	87.396	33.266
2	85.234	30.026	86.017	31.641	83.542	28.692	84.338	4.0066	85.973	32.261	87.397	33.268
3	85.270	30.040	85.984	31.624	83.519	28.700	84.328	4.0238	85.973	32.273	87.397	33.263
4	85.251	30.033	86.010	31.655	83.547	28.722	84.337	3.9856	85.982	32.277	87.392	33.259
5	85.228	30.039	86.022	31.653	83.512	28.694	84.330	4.017	85.977	32.266	87.398	33.271
6	85.260	30.038	86.019	31.650	83.546	28.690	84.335	4.028	85.989	32.297	87.398	33.275
7	85.256	30.035	86.019	31.610	83.496	28.674	84.343	3.995	85.979	32.271	87.396	33.268
8	85.243	30.028	86.012	31.655	83.540	28.707	84.336	3.988	85.968	32.268	87.390	33.267
9	85.246	30.037	86.018	31.638	83.565	28.724	84.331	3.975	85.967	32.266	87.393	33.272
10	85.253	30.034	85.996	31.659	83.524	28.696	84.338	4.010	85.962	32.276	87.396	33.266
Best	85.228	30.026	85.985	31.624	83.496	28.674	84.328	3.9753	85.962	32.261	87.390	33.259
Worst	85.270	30.040	86.022	31.661	83.565	28.724	84.343	4.0415	85.989	32.297	87.398	33.275
Mean	85.248	30.035	86.010	31.648	83.531	28.699	84.336	4.0070	85.974	32.272	87.395	33.268
Median	85.249	30.036	86.014	31.652	83.532	28.695	84.337	4.0080	85.974	32.269	87.396	33.267
StD	0.013	0.0049	0.012	0.0113	0.0205	0.0150	0.0047	0.0211	0.0078	0.010	0.0028	0.0046
Run	Daily cost (c€)	Cost per kW (c€/kW)	Daily cost (c€)	Cost per kW (c€/kW)	Daily cost (c€)	Cost per kW (c€/kW)	Daily cost (c€)	Cost per kW (c€/kW)	Daily cost (c€)	Cost per kW (c€/kW)	Daily cost (c€)	Cost per kW (c€/kW)
1	1,732,174	0.2316	1,268,355	0.1685	2,426,193	0.3261	3,102,432	0.2453	1,493,717	0.1980	1,194,906	0.1576
2	1,730,007	0.2313	1,268,809	0.1686	2,421,798	0.3255	3,104,940	0.2455	1,494,695	0.1981	1,194,381	0.1577
3	1,734,499	0.2319	1,268,476	0.1685	2,422,010	0.3255	3,103,108	0.2453	1,494,752	0.1981	1,194,523	0.1577
4	1,733,342	0.2317	1,269,484	0.1687	2,423,270	0.3257	3,100,843	0.2452	1,495,670	0.1983	1,194,541	0.1577
5	1,731,563	0.2315	1,269,444	0.1687	2,425,343	0.3260	3,102,625	0.2453	1,495,056	0.1982	1,194,662	0.1577
6	1,731,723	0.2315	1,268,433	0.1685	2,421,875	0.3255	3,101,560	0.2452	1,495,345	0.1982	1,194,988	0.1578
7	1,729,291	0.2312	1,268,855	0.1686	2,423,328	0.3257	3,103,369	0.2454	1,495,925	0.1983	1,194,602	0.1577
8	1,733,356	0.2316	1,269,636	0.1687	2,425,034	0.3259	3,104,131	0.2454	1,495,928	0.1983	1,194,808	0.1577
9	1,730,956	0.2314	1,268,540	0.1685	2,420,079	0.3252	3,102,209	0.2453	1,492,750	0.1979	1,194,559	0.1577
10	1,734,204	0.2319	1,268,898	0.1686	2,419,501	0.3252	3,102,144	0.2453	1,494,011	0.1980	1,194,906	0.1578
Best	1,729,291	0.2312	1,268,355	0.1685	2,419,501	0.3252	3,100,843	0.2452	1,492,750	0.1979	1,194,381	0.158
Worst	1,734,499	0.2319	1,269,636	0.1686	2,426,193	0.3261	3,104,940	0.2455	1,495,928	0.1983	1,194,988	0.1578
Mean	1,732,112	0.2316	1,268,893	0.1686	2,422,843	0.3256	3,102,736	0.2453	1,494,785	0.1981	1,194,688	0.1577
Median	1,731,949	0.2315	1,268,832	0.1686	2,422,640	0.3256	3,102,529	0.2453	1,494,904	0.1982	1,194,632	0.1577
StD	1742.177	$23 \cdot 10^{-4}$	472.933	$6 \cdot 10^{-4}$	2216657.4	$30 \cdot 10^{-4}$	1203.793	$9 \cdot 10^{-4}$	1036.363	$13 \cdot 10^{-4}$	202.001	$2 \cdot 10^{-4}$
Effi	68.09		93.54		48.42		64.28		79.58		99.97	

Table 6
ANOVA table.

Source	SS	df	MS	*F*	*p*-value
Columns (between)	0.18927	5	0.03785 e−08	1.28745e6	9.82601×10^{-136}
Error (within)	1.58772	54	2.94021		
Total	0.18927	59			

performance was similar for all optimizers. This can be interpreted by the fact that a flat controller was an independent unit, thus, the optimizer did not have a considerable impact on its performance. Nevertheless, the flat controller performance was still excellent.

6. Conclusion and future work

An efficient energy management strategy (EMS) for the economic operation of a microgrid under standalone and grid-connected operating modes was proposed. The proposed EMS technique was based on the bald eagle search optimization algorithm (BES). Three goals were achieved: the first was to satisfy the load power with the lowest operating costs under a stable direct current (DC) bus voltage, second: was to enhance the overall system efficiency and lastly: the third goal was to protect the battery from deep discharge and overcharge. To prove the superiority of the proposed energy management strategy, the obtained results were compared with other optimizers, including particle swarm optimization, salp swarm algorithm, artificial eco-system optimizer, COOT optimizer, and political optimizer. The minimum operating energy cost (0.1577c€/kW), superior efficiency (87.395%), and raised final state of charge (33.268%) were achieved thanks to the proposed energy management strategy, based on the bald eagle search optimization algorithm. Thus, as a conclusion, the proposed EMS effectively responded to the predetermined objectives.

In our future works, we aim to combine the energy management strategy and the flat controller by including the controller parameters in the optimizer as optimization variables. For this, the objective function has to include the voltage error or use a multi-objective optimization algorithm. Moreover, hardware in the loop (HIL) may be performed in our future works to resolve the BES algorithm's high complexity.

Declaration of Competing Interest

The authors declare that they have no known competing financial interests or personal relationships that could have appeared to influence the work reported in this paper.

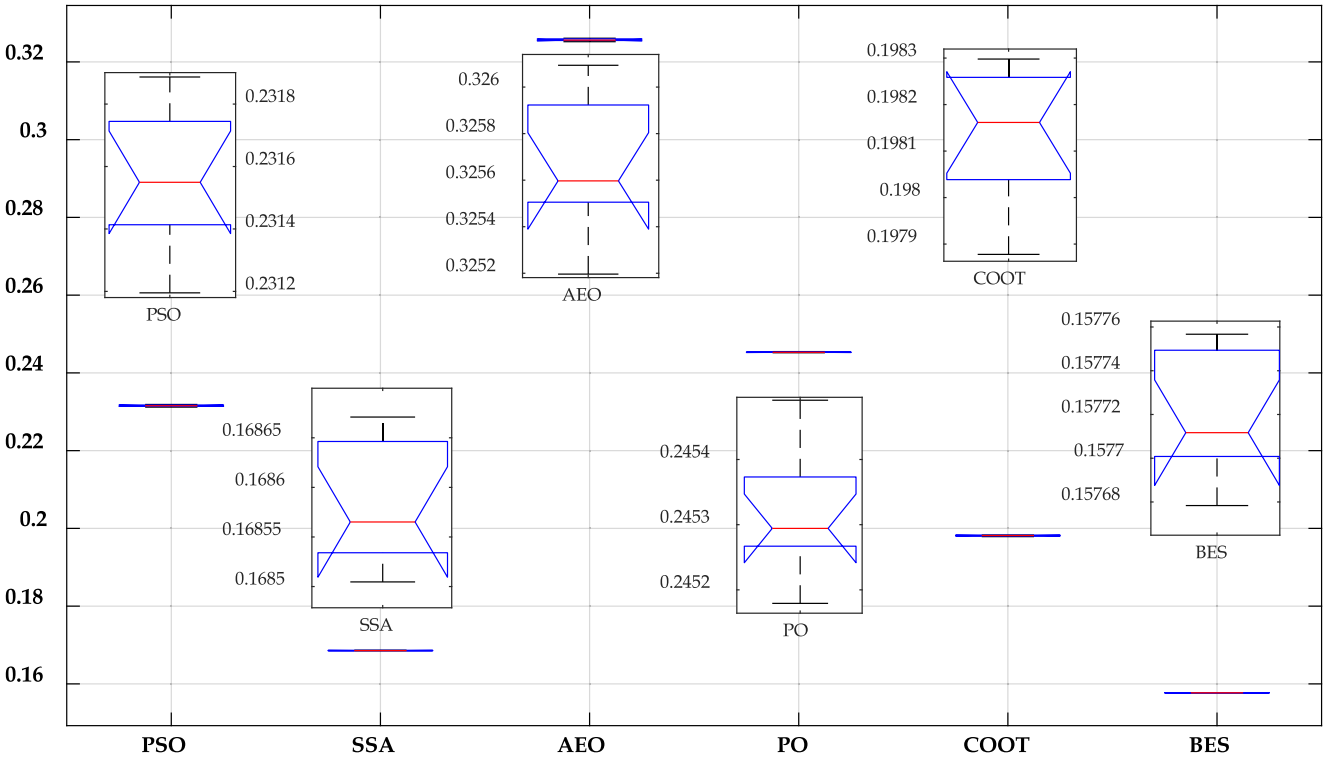

Fig. 12. ANOVA graphical ranking results.

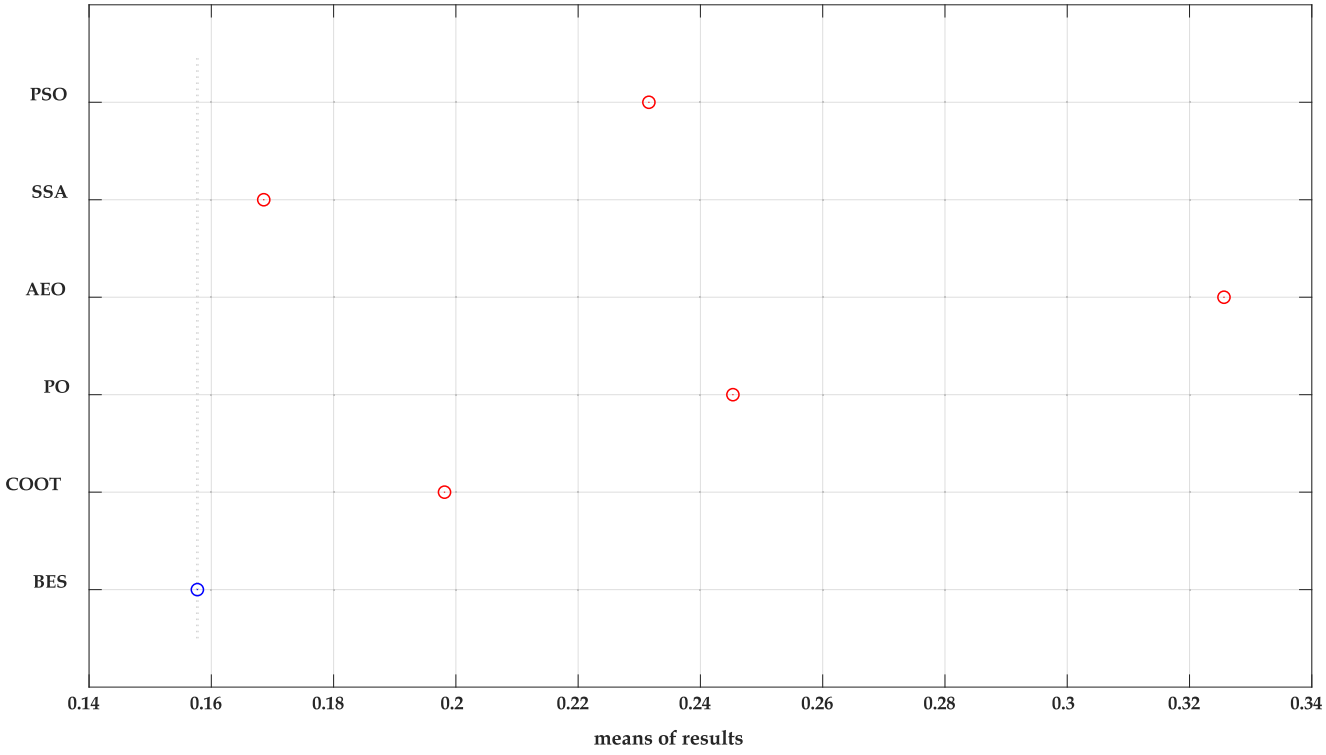

Fig. 13. Tukey HSD test results.

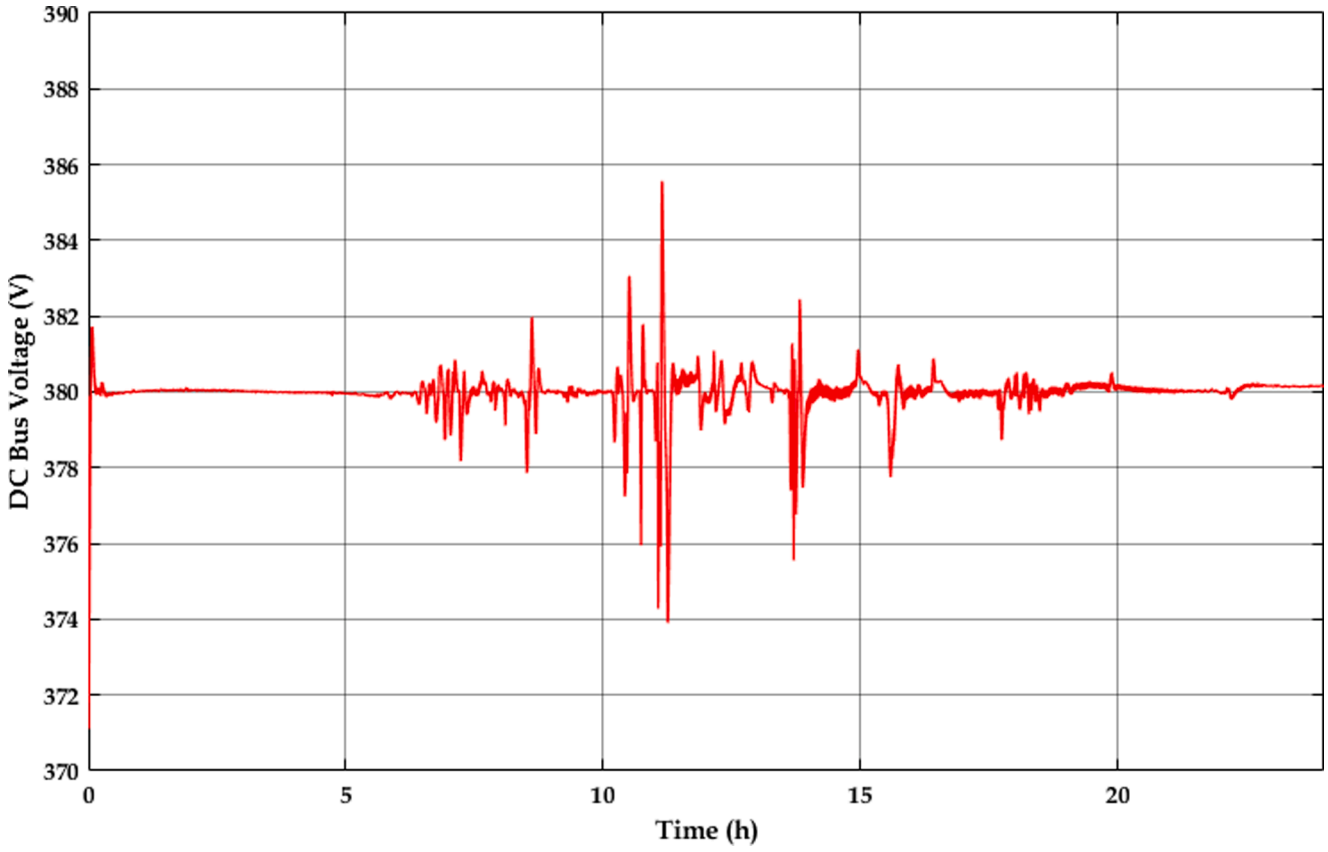

Fig. 14. The DC bus voltage applying the proposed flat controller (V).

Table 7
Statistics on the DC bus voltage.

	PSO	SSA	AEO	PO	COOT	BES
min	371.0675	371.1028	371.0677	371.1081	371.1039	371.0988
max	385.4200	385.7237	385.0700	386.5195	385.5655	386.3551
mean	379.9854	379.9853	379.9856	379.9855	379.9857	379.9855
median	380.0259	380.0234	380.0276	380.0243	380.0197	380.0243
mode	371.0675	371.1028	371.0677	371.1081	371.1039	371.0988
std	0.5652	0.5872	0.5443	0.6398	0.5767	0.6224
range	14.352	14.6209	14.0022	15.4114	14.4616	15.2563

Appendix A

A.1. Flatness control equations

From Eq. (12), the required power by the common bus (E_{bus}^{req}) can be obtained as

$$\frac{d(E_{bus}-E_{bus}^{ref})}{dt}=k_1(E_{bus}^{ref}-E_{bus})+k_2\int_0^t(E_{bus}^{ref}-E_{bus})dt \tag{30}$$

For a constant DC bus reference voltage

$$\frac{d(E_{bus}^{ref})}{dt}=\frac{d(C_{bus}E_{bus}^{ref}/2)}{dt}=0 \tag{31}$$

Then

$$\dot{E}_{bus}^{req}=\frac{d(E_{bus})}{dt}=k_1(\varepsilon_{bus})+k_2\int_0^t(\varepsilon_{bus})dt$$
$$\varepsilon_{bus}=E_{bus}^{ref}-E_{bus} \tag{32}$$

Replacing in Eq. (11)

$$P_{Batt}^{ref}=(k_1(\varepsilon_{bus})+k_2\int_0^t(\varepsilon_{bus})dt)+P_{Load}-P_{PV}-P_{FC}-P_{Grid} \tag{33}$$

A.2. AEO

Following Eq. (23), If the living is a carnivore

$$\begin{cases} x_i^{t+1} = x_i^t + C(x_i^t - x_j^t), \quad i \in [3, ..n] \\ j = randi([2 \quad i-1]) \end{cases} \tag{34}$$

If the living is an omnivore

$$\begin{cases} x_i^{t+1} = x_i^t + C(r_2(x_i^t - x_j^t) + (1-r_2)(x_i^t - x_j^t)) \quad i \in [3, ..n] \\ j = randi([2 \quad i-1]) \end{cases} \tag{35}$$

The decomposition' model is presented as

$$\begin{aligned} x_i^{t+1} &= x_n^t + D(ex_n^t - hx_i^t), \quad i \in [1, ..n] \\ D &= 3u, \quad u \sim N(0,1) \\ e &= r_3.randi([1 \quad 2]) - 1 \\ h &= 2r_3^{AEO} - 1 \end{aligned} \tag{36}$$

where $r_3^{AEO}$is a random number [0, 1].

A.3. The optimizer average efficiency

The average efficiency is estimated based on the following relation:

$$\eta_{av} = \frac{100}{n}\sum_{i=1}^{n}\frac{OF_{nom}}{OF_{est}} \tag{37}$$

where n is the number of runs, OF_{est} is the estimated fitness function, and OF_{nom} is the nominal objective function.

A.4. ANOVA table

Source	Sums of Squares (SS)	df	Mean Squares (MS)	F
Between	$SSB = \sum n_j(\overline{X} - \overline{X}_j)^2$	k-1	$MSB = \frac{SSB}{k-1}$	$F = \frac{SSE}{MSE}$
Error	$SSE = \sum\sum(\overline{X} - \overline{X}_j)^2$	N-k	$MSE = \frac{SSE}{N-k}$	
Total	$SST = \sum\sum(\overline{X} - \overline{X}_j)^2$	N-1		

$\overline{X}_j$: Sample mean of the j-th group.
$\overline{X}$: Overall sample mean of all groups.
k: the number of independent groups.
N: The total number of sample size.

A.5. Tukey test

$$\begin{aligned} q &= \frac{\overline{X}_{max} - \overline{X}_{min}}{s.e} \\ e &= \sqrt{2/n} \end{aligned} \tag{38}$$

$\overline{X}_{max}$: The largest sample means.
$\overline{X}_{min}$: The smallest sample means.
s^2: The pooled sample variance from these samples.
n: Size of the samples.

References

[1] Wei C, Shen Z, Xiao D, Wang L, Bai X, Chen H. An optimal scheduling strategy for peer-to-peer trading in interconnected microgrids based on RO and Nash bargaining. Appl Energy 2021;295:117024. https://doi.org/10.1016/j.apenergy.2021.117024.

[2] Pascual J, Arcos-Aviles D, Ursúa A, Sanchis P, Marroyo L. Energy management for an electro-thermal renewable–based residential microgrid with energy balance forecasting and demand side management. Appl Energy 2021;295:117062. https://doi.org/10.1016/j.apenergy.2021.117062.

[3] Boza P, Evgeniou T. Artificial intelligence to support the integration of variable renewable energy sources to the power system. Appl Energy 2021;290:116754. https://doi.org/10.1016/j.apenergy.2021.116754.

[4] Zia MF, Elbouchikhi E, Benbouzid M. Microgrids energy management systems: A critical review on methods, solutions, and prospects. Appl Energy 2018;222:1033–55. https://doi.org/10.1016/j.apenergy.2018.04.103.

[5] Li Y, Miao S, Luo X, Yin B, Han Ji, Wang J. Dynamic modelling and techno-economic analysis of adiabatic compressed air energy storage for emergency back-up power in supporting microgrid. Appl Energy 2020;261:114448. https://doi.org/10.1016/j.apenergy.2019.114448.

[6] Boretti A. Advantages and Disadvantages of Diesel Single and Dual-Fuel Engines. Front Mech Eng 2019;5:64. https://doi.org/10.3389/fmech.2019.00064.
[7] Zhang C, Greenblatt JB, Wei M, Eichman J, Saxena S, Muratori M, et al. Flexible grid-based electrolysis hydrogen production for fuel cell vehicles reduces costs and greenhouse gas emissions. Appl Energy 2020;278:115651. https://doi.org/10.1016/j.apenergy.2020.115651.
[8] Yuan M, Fu Y, Mi Y, Li Z, Wang C. Hierarchical control of DC microgrid with dynamical load power sharing. Appl Energy 2019;239:1–11. https://doi.org/10.1016/j.apenergy.2019.01.081.
[9] dos Santos Neto PJ, Barros TAS, Silveira JPC, Ruppert Filho E, Vasquez JC, Guerrero JM. Power management techniques for grid-connected DC microgrids: A comparative evaluation. Appl Energy 2020;269:115057. https://doi.org/10.1016/j.apenergy.2020.115057.
[10] Tooryan F, HassanzadehFard H, Collins ER, Jin S, Ramezani B. Smart integration of renewable energy resources, electrical, and thermal energy storage in microgrid applications. Energy 2020;212:118716. https://doi.org/10.1016/j.energy.2020.118716.
[11] Malik SM, Sun Y, Huang W, Ai X, Shuai Z. A Generalized Droop Strategy for Interlinking Converter in a Standalone Hybrid Microgrid. Appl Energy 2018;226:1056–63. https://doi.org/10.1016/j.apenergy.2018.06.002.
[12] Kaluthanthrige R, Rajapakse AD. Evaluation of hierarchical controls to manage power, energy and daily operation of remote off-grid power systems. Appl Energy 2021;299:117259. https://doi.org/10.1016/j.apenergy.2021.117259.
[13] Cavraro G, Caldognetto T, Carli R, Tenti P. A Master/Slave Approach to Power Flow and Overvoltage Control in Low-Voltage Microgrids. Energies 2019;12:2760. https://doi.org/10.3390/en12142760.
[14] Radosavljevic J. Metaheuristic Optimization in Power Engineering. London: Institution of Engineering and Technology; 2018. https://doi.org/10.1049/pbpo131e.
[15] Wang C, Nehrir MH. Power Management of a Standalone Wind/Photovoltaic/Fuel Cell Energy System. IEEE Trans Energy Convers 2008;23:957–67. https://doi.org/10.1109/TEC.2007.914200.
[16] Bartolucci L, Cordiner S, Mulone V, Rossi JL. Hybrid renewable energy systems for household ancillary services. Int J Electr Power Energy Syst 2019;107:282–97. https://doi.org/10.1016/j.ijepes.2018.11.021.
[17] Onar OC, Uzunoglu M, Alam MS. Modeling, control and simulation of an autonomous wind turbine/photovoltaic/fuel cell/ultra-capacitor hybrid power system. J Power Sources 2008;185(2):1273–83. https://doi.org/10.1016/j.jpowsour.2008.08.083.
[18] Gonzalez-Garrido A, Saez-de-Ibarra A, Milo A, Gaztanaga H, Eguia P. Techno-Economic Assessment of Energy Management Strategies for a Renewable Portfolio with Storage Systems in Energy and Frequency Reserve Markets. In: IEEE, 2019; 2019. p. 1–6. https://doi.org/10.1109/EEM.2019.8916445.
[19] Hatziargyriou ND, Anastasiadis AG, Tsikalakis AG, Vasiljevska J. Quantification of economic, environmental and operational benefits due to significant penetration of Microgrids in a typical LV and MV Greek network. Eur Trans Electr Power 2011;21:1217–37. https://doi.org/10.1002/etep.392.
[20] García P, Torreglosa JP, Fernández LM, Jurado F, Langella R, Testa A. Energy management system based on techno-economic optimization for microgrids. Electr Power Syst Res 2016;131:49–59. https://doi.org/10.1016/j.epsr.2015.09.017.
[21] Mohamed FA, Koivo HN. Online management genetic algorithms of microgrid for residential application. Energy Convers Manag 2012;64:562–8. https://doi.org/10.1016/j.enconman.2012.06.010.
[22] Moghaddam AA, Seifi A, Niknam T, Alizadeh Pahlavani MR. Multi-objective operation management of a renewable MG (micro-grid) with back-up micro-turbine/fuel cell/battery hybrid power source. Energy 2011;36(11):6490–507. https://doi.org/10.1016/j.energy.2011.09.017.
[23] Li Peng, Weina Xu, Zhou Zeyuan, Li Rui. Optimized operation of microgrid based on gravitational search algorithm. In: . 2013 Int. Conf. Electr. Mach. Syst. IEEE; 2013. p. 338–42. https://doi.org/10.1109/ICEMS.2013.6754475.
[24] Ferahtia Seydali, Djeroui Ali, Rezk Hegazy, Houari Azeddine, Zeghlache Samir, Machmoum Mohamed. Optimal Control and Implementation of Energy Management Strategy for a DC Microgrid. Energy 2022;238:121777. https://doi.org/10.1016/j.energy.2021.121777.
[25] Ferahtia Seydali, Djeroui Ali, Mesbahi Tedjani, Houari Azeddine, Zeghlache Samir, Rezk Hegazy, et al. Optimal Adaptive Gain LQR-Based Energy Management Strategy for Battery-Supercapacitor Hybrid Power System. Energies 2021;14(6):1660. https://doi.org/10.3390/en14061660.
[26] Ferahtia S, Djerioui A, Zeghlache S, Houari A. A hybrid power system based on fuel cell, photovoltaic source and supercapacitor. SN Appl Sci 2020;2:940. https://doi.org/10.1007/s42452-020-2709-0.
[27] Alsattar HA, Zaidan AA, Zaidan BB. Novel meta-heuristic bald eagle search optimisation algorithm. Artif Intell Rev 2020;53(3):2237–64. https://doi.org/10.1007/s10462-019-09732-5.
[28] Kiranyaz S. Particle swarm optimization. Adapt Learn Optim 2014;15:45–82. https://doi.org/10.1007/978-3-642-37846-1_3.
[29] Mirjalili S, Gandomi AH, Mirjalili SZ, Saremi S, Faris H, Mirjalili SM. Salp Swarm Algorithm: A bio-inspired optimizer for engineering design problems. Adv Eng Softw 2017;114:163–91. https://doi.org/10.1016/j.advengsoft.2017.07.002.
[30] Zhao Weiguo, Wang Liying, Zhang Zhenxing. Artificial ecosystem-based optimization: a novel nature-inspired meta-heuristic algorithm. Neural Comput Appl 2020;32(13):9383–425. https://doi.org/10.1007/s00521-019-04452-x.
[31] Askari Qamar, Younas Irfan, Saeed Mehreen. Political Optimizer: A novel socio-inspired meta-heuristic for global optimization. Knowledge-Based Syst 2020;195:105709. https://doi.org/10.1016/j.knosys.2020.105709.
[32] Naruei Iraj, Keynia Farshid. A New Optimization Method Based on Coot Bird Natural Life Model. Expert Syst Appl 2021;183:115352. https://doi.org/10.1016/j.eswa.2021.115352.